ACS APPLIED MATERIALS & INTERFACES

Research Article

www.acsami.org

Crystal-Site Engineering Control for the Reduction of Eu^{3+} to Eu^{2+} in $CaYAlO_4$: Structure Refinement and Tunable Emission Properties

Yang Zhang,[†,‡] Xuejiao Li,[†] Kai Li,[†,‡] Hongzhou Lian,[†] Mengmeng Shang,*[,†] and Jun Lin*[,†]

[†]State Key Laboratory of Rare Earth Resource Utilization, Changchun Institute of Applied Chemistry, Chinese Academy of Sciences, Changchun 130022, People's Republic of China

[‡]University of the Chinese Academy of Sciences, Beijing 100049, People's Republic of China

Supporting Information

ABSTRACT: In this article, Eu-activated $CaYAlO_4$ aluminate phosphors were synthesized by a solid-state reaction. Under UV light excitation, characteristic red line emission of Eu^{3+} was detected in the range of 570−650 nm. In addition, we introduced crystal-site engineering approach into the $CaYAlO_4$ host through incorporation of Si^{4+}−Ca^{2+} to replace Al^{3+}−Y^{3+}, which would shrink the AlO_6 octahedrons, accompanied by the expansion of CaO_9 polyhedron, and then enable the partial reduction of Eu^{3+} to Eu^{2+}. The crystal structure and underlying mechanism have been clarified on the basis of the Rietveld refinement analysis. The PL spectra of $Ca_{0.99+x}Y_{1-x}Al_{1-x}Si_xO_4{:}Eu_{0.01}$ (x = 0−0.30) exhibit both green emission of Eu^{2+} ($4f^65d^1$−$4f^7$, broadband around 503 nm) and red-orange emission of Eu^{3+} ($^5D_0$−$^7F_{1,2}$, 593 and 624 nm) under UV light excitation with a quantum yield of 38.5%. The CIE coordinates of $Ca_{0.99+x}Y_{1-x}Al_{1-x}Si_xO_4{:}Eu_{0.01}$ (x = 0−0.30) phosphors are regularly shifted from (0.482, 0.341) to (0.223, 0.457) with increasing x, which would expand the application of Eu. Furthermore, this investigation reveals the correlations of structure and property of luminescent materials, which would shed light on the development of novel phosphors suitable for lighting and display applications.

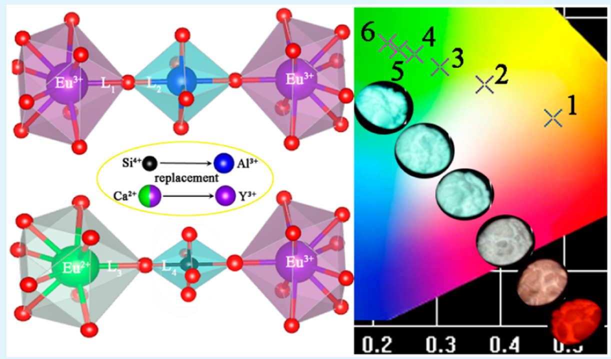

KEYWORDS: *WLEDs, phosphors, crystal-site engineering, structure and property, Rietveld refinement, tunable emission*

1. INTRODUCTION

Recently, light-emitting diodes (LEDs), as one promising solid-state lighting (SSL) technique, are a viable option to overtake traditional incandescent or fluorescence lamps on the illumination, due to their small size, eco-friendliness, energy savings, high brightness, and a long lifetime.[1−10] As compared to the all-LED devices, phosphors-converted white LEDs (pc-WLEDs) have attracted much attention due to their fascinating merits, such as high color rendering index (CRI), high stability, and easy tunability of color temperatures.[4,7,11] Thus, the characteristic properties of the phosphors, including photoluminescence excitation (PLE) and emission wavelengths, thermal stability, and quantum efficiency, play a critical role in determine the luminous efficacy, color temperature, and color rendition of the WLEDs. It is essential to design some efficient phosphors for practical applications.[12−16]

Rare-earth ions, as widely used activators, have been playing an irreplaceable role in modern lighting and display fields due to their abundant emission colors based on the 4f−4f or 5d−4f transitions.[17−23] Especially, Eu is the most commonly used activator because both Eu^{3+} and Eu^{2+} can function as an emission center in the host lattices.[24−27] As one of the most frequently used red-emitting activators, Eu^{3+} ions mainly show characteristic emissions resulting from the transitions of $^5D_0$−^7F_J (J = 0,...,4). In addition, it is also possible to obtain simultaneously the red emission from the $^5D_0$ level and the blue and green emissions from the higher ^5D levels ($^5D_1$, $^5D_2$, and $^5D_3$) of Eu^{3+} through delicately selecting the host lattice and doping concentration of Eu^{3+}, resulting in a white light emission from Eu^{3+} singly doped phosphors.[26,28−30] While the line emission (full width at half-maximum, fwhm) and color characteristics of Eu^{3+} ions are promising for WLEDs, the parity-forbidden 4f−4f transitions have low oscillator strength (about 10^{-6}), resulting in low absorption efficiency and low CRI.[2,3] Considering that the 4f−5d transitions of Eu^{2+} ion are parity-allowed, Eu^{2+} activated phosphors usually have a broad excitation band and tunable emission colors ranging from blue to deep red, which is more suitable for application in WLEDs.[31−34] However, less research has been conducted on the reduction of Eu^{3+} through crystal-site engineering approach by modifying the coordination environment and crystal site size of activators, to then fulfill the coexistence of luminescence from Eu^{3+} and Eu^{2+} in single phased phosphors.[11,12,35,36] Accordingly, it is a promising method to overcome the limitations of Eu^{3+} activated phosphors via valence transfer,

Received: November 6, 2014
Accepted: January 15, 2015
Published: January 15, 2015

DOI: 10.1021/am508859c
ACS Appl. Mater. Interfaces 2015, 7, 2715−2725

combined with the luminescence of Eu^{2+} to obtain warm white light.

The aluminate $CaYAlO_4$ with the K_2NiF_4 structure has aroused great interest as a host for luminescent materials.[37−41] However, all of the reported results are focused on the luminescent properties of Ln^{3+}-doped (Ln = Eu, Tb, Er, Ce, and Yb) $CaYAlO_4$, such as Tb^{3+}/Eu^{3+} for field emission displays, Ce^{3+}/Pr^{3+} for quantum-cutting, and Er^{3+}/Yb^{3+} for up-conversion.[37,38,42] To the best of our knowledge, there are no reports about Eu^{2+}-doped $CaYAlO_4$. This is mainly because of the highly compressed Ca^{2+} sites in the framework of $CaYAlO_4$, in which the CaO_9 polyhedrons are surrounded compactly by AlO_6 octahedrons. As a result, it is difficult to obtain Eu^{2+} emission in $CaYAlO_4$ through conventional high temperature solid-state reaction under a reducing atmosphere. Herein, we demonstrate the feasibility of transforming Eu^{3+}-activated $CaYAlO_4$ into Eu^{2+} or mix Eu^{3+}/Eu^{2+} activated phosphors through crystal-site engineering approach by incorporation of $Si^{4+}-Ca^{2+}$ in the host materials. The active site is gradually expanded by the substitution of $Al^{3+}-Y^{3+}$ by $Si^{4+}-Ca^{2+}$ in $CaYAlO_4$:Eu system, which is critical for the reduction of Eu^{3+} to Eu^{2+} because the radius of Eu^{2+} is larger. The underlying mechanism has been clarified by the Rietveld refinement analysis. The obtained $Ca_{0.99+x}Y_{1-x}Al_{1-x}Si_xO_4:Eu_{0.01}$ (x = 0−0.30) phosphors present not only a broad PLE spectrum (ranging from 250 to 450 nm) but also tunable luminescence (Eu^{2+} and Eu^{3+}), which holds great promise for application in WLEDs.

2. EXPERIMENTAL SECTION

Materials. $CaCO_3$, Al_2O_3, and SiO_2 were purchased from Sigma-Aldrich. The Y_2O_3, Eu_2O_3 (99.999%) was purchased from Science and Technology Parent Co. of Changchun Institute of Applied Chemistry. All chemicals were used directly without further purification.

Preparation. $Ca_{0.99+x}Y_{1-x}Al_{1-x}Si_xO_4:Eu_{0.01}$ (x = 0−0.30) powder samples were prepared by the conventional solid-sstate reaction process from $CaCO_3$, Al_2O_3, SiO_2, Y_2O_3, and Eu_2O_3. First, the stoichiometry contents of reagents were ground in an agate mortar for 30 min for a good mixing. The mixture was calcined in aluminum oxide crucible at 1200 °C for 6 h under a reducing atmosphere of H_2 (10%) and N_2 (90%). The sintered samples were ground for 45 min to form a homogeneous mixture. The mixture then was fired again at 1500−1600 °C for 6 h under a reducing atmosphere of H_2 (10%) and N_2 (90%), yielding the resulting phosphors.

Characterization. The X-ray diffraction (XRD) measurements were performed on a D8 Focus diffractometer in the 2θ range from 10° to 100° operating at 40 kV and 40 mA with graphite-monochromatized Cu Kα radiation (λ = 0.15405 nm). The Rietveld analysis of the XRD was done using the General Structure Analysis System (GSAS) program.[43] Transmission electron microscopy (TEM) images were recorded using a FEI Tecnai G2S-Twin with a field-emission gun operating at 200 kV. Images were acquired digitally on a Gatan multipole CCD camera. Raman spectrum was collected using a micro-Raman spectrometer with a laser of 532 nm wavelength. XPS spectra were measured with a Thermo ESCALAB 250 instrument. Solid-state nuclear magnetic resonance (NMR) spectra were acquired on a 400 MHz AVANCE III wide bore NMR spectrometer equipped with a 4 mm rotor. The photoluminescence (PL) measurements were recorded with a Hitachi F-7000 spectrophotometer equipped with a 150 W xenon lamp as the excitation source. Photoluminescence absolute quantum yields (QY) were measured by an absolute PL quantum yield measurement system (C9920-02, Hamamatsu Photonics K. K., Japan). Time-resolved photoluminescence spectra and luminescence decay curves were obtained from a Lecroy Wave Runner 6100 Digital oscilloscope (1 GHz) (pulse width = 4 ns, gate = 50 ns) as the excitation source (Continuum Sunlite OPO). All of the measurements were performed at room temperature (RT).

3. RESULTS AND DISCUSSION

The XRD pattern of the $CaYAlO_4:0.01Eu^{3+}$ was first refined by the General Structure Analysis System (GSAS) program implemented with the starting model built with isostructure information reported by previous research.[37,43,44] Figure 1a presents the observed, calculated, Bragg positions and the difference patterns of the XRD refinement of $CaYAlO_4:0.01Eu^{3+}$ sample, respectively. The obtained converged weighted-profiles of R_p = 5.42% and R_{wp} = 8.01% reveal a good quality of fit. However, we can see a minor impurity peak at 29−30° in the enlarged XRD pattern shown in Supporting Information Figure S1, which can be assigned to hexagonal Y_2O_3. Considering the fact that the content of Y_2O_3 is extremely low (<1%) and it has no effect on the luminescence of Eu^{2+}, it was included in the refinement as displayed in Figure 1a. Thus, the attention is focused on the variation of crystal structure and photoluminescence properties of the dominant phase $CaYAlO_4$. The TEM images obtained from the selected $CaYAlO_4:0.01Eu^{3+}$ sample have been measured and are shown in Supporting Information Figure S2. The fine structures are further examined by HRTEM and the fast Fourier transform (FFT) images as presented in Supporting Information Figure S2b and c. The selected area electron diffraction (SAED) pattern in Supporting Information Figure S2d shows strong concentric ring patterns that can be indexed to the (101), (103), and (112) planes of $CaYAlO_4$, respectively, indicating the high crystalline nature of the sample. As the crystallographic data of $CaYAlO_4:0.01Eu^{3+}$ shown in Table 1, this aluminate

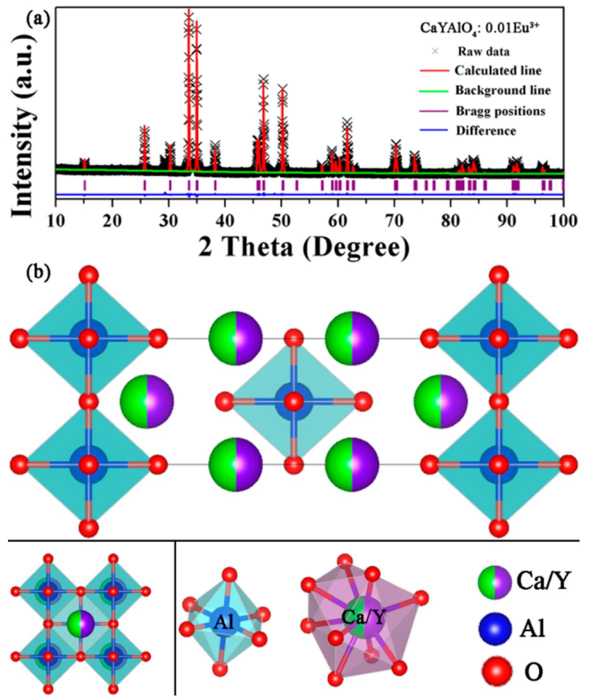

Figure 1. (a) Experimental (cross), calculated (solid line), and difference (bottom) results of powder X-ray diffraction (XRD) refinements of $CaYAlO_4:0.01Eu^{3+}$. Bragg reflections are indicated with tick marks. (b) Typical crystal structure of $CaYAlO_4$ and the Al^{3+} and Ca^{2+}/Y^{3+} sites are depicted with six- and nine-coordination with oxygen atoms, respectively.

Table 1. Crystallographic Data of $CaYAlO_4$:0.01Eu^{3+}, As Determined by the Rietveld Refinement of Powder XRD Data at Room Temperature[a]

atom	site	x	y	z	occupancy
Ca1	4e	0.0000	0.0000	0.3591	0.495
Y1	4e	0.0000	0.0000	0.3591	0.500
Al1	2a	0.0000	0.0000	0.0000	1.000
O1	4c	0.0000	0.5000	0.0000	1.000
O2	4e	0.0000	0.0000	0.1693	1.000
Eu1	4e	0.0000	0.0000	0.3591	0.005

[a]Tetragonal crystal system, space group: *I*4/*mmm* (No. 139), *Z* = 2, $a = b = 3.64766$ Å, $c = 11.88495$ Å, $V = 158.13$ Å^3, $\alpha = \beta = \gamma = 90°$, $R_p = 5.42\%$, $R_{wp} = 8.01\%$.

compound has a tetragonal crystal system with space group *I*4/*mmm* (No. 139), *Z* = 2, and the lattice constants are determined to be $a = b = 3.64766$ Å, $c = 11.88495$ Å, $V = 158.13$ Å^3, which is consistent with previous reports.[37,44] In the typical crystal structure of $CaYAlO_4$ shown in Figure 1b, the Al atoms occupy the 2*a* site coordinated by six O atoms to form AlO_6 octahedron. The Ca and Y atoms are both expected to occupy the 4*e* site randomly keeping the composition ratio of 1:1 in the center of $(Ca/Y)O_9$ polyhedron. O atoms are distributed over the 4*c* site and the 4*e* site, denoted as O1 and O2, respectively. The crystal structure of $CaYAlO_4$ can be described as a highly condensed framework of AlO_6 octahedrons and $(Ca/Y)O_9$ polyhedrons sharing the O^{2-} vertexes. Notably, the $(Ca/Y)O_9$ polyhedron is closely surrounded by AlO_6 octahedrons to form a cage structure.[37] Thus, it can be concluded that the local environment of Ca/Y sites is highly compressed due to the rigid structure of $CaYAlO_4$, which gives rise to the difficulty of reduction of Eu^{3+} activators.[12,45,46]

Figure 2 describes the photoluminescence excitation (PLE) and emission (PL) spectra of $CaYAlO_4$:0.01Eu^{3+} with the schematic energy levels. The PLE spectrum monitored at 624 nm reveals a broad band in the range of 200−350 nm due to the charge transfer band (CTB) of O−Eu, along with some weak peaks in the range of 350−500 nm related to the 4f−4f transitions of Eu^{3+} ions.[37] Under the excitation of 277 nm, the sharp emission lines of $CaYAlO_4$:0.01Eu^{3+} can be assigned to Judd−Ofelt transitions ($^5D_{0,1,2,3}$−^7F_J) of Eu^{3+}, that is, $^5D_3$−$^7F_1$ (420 nm), $^5D_3$−$^7F_2$ (430 nm), $^5D_3$−$^7F_3$ (448 nm), $^5D_2$−$^7F_0$ (469 nm), $^5D_2$−$^7F_2$ (490 nm), $^5D_2$−$^7F_3$ (515 nm), $^5D_1$−$^7F_1$ (540 nm), $^5D_1$−$^7F_2$ (555 nm), $^5D_0$−$^7F_1$ (593 nm), and $^5D_0$−$^7F_2$ (624 nm), indicating that an efficient phonon-assisted process leads to the relaxation from CTB to Eu^{3+} energy levels.[25] Furthermore, the electric dipole transition ($^5D_0$−$^7F_2$, 624 nm) is stronger than the magnetic dipole transition ($^5D_0$−$^7F_1$, 593 nm), indicating that the Eu^{3+} ions mainly occupy the sites without or deviated from inversion symmetry, basically agreeing with the coordination environment of Ca/Y presented in Figure 1b.[47] The corresponding Commission International de I'Eclairage (CIE) chromaticity coordinate is determined to be (0.503, 0.350), which is located in the red-orange zone as the photograph shows in Figure 2. While the line emission (fwhm about 4 nm) and color characteristics of Eu^{3+} ions are promising for solid-state lighting, the parity-forbidden 4f−4f transitions have low oscillator strength (about 10^{-6}), resulting in low absorption efficiency in the NUV and blue light. Thus, Eu^{3+}-activated materials are difficult to apply in pc-WLEDs because line emission yields a rather low CRI and weak absorption in NUV or blue-LEDs.[2,12,48]

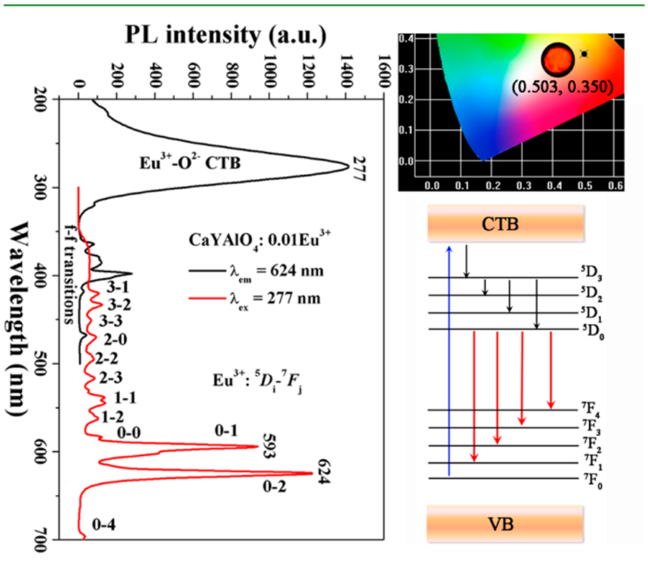

Figure 2. PLE and PL spectra of $CaYAlO_4$:0.01Eu^{3+} sample (λ_{em} = 624 nm, λ_{ex} = 277 nm) with corresponding photograph, CIE coordinates, and schematic energy level of Eu^{3+}.

As the PL spectrum and photograph show in Figure 2, it is obvious that Eu^{3+} could not be directly reduced to Eu^{2+} in $CaYAlO_4$:Eu^{3+} system under a reducing atmosphere. Considering the effect of local unbalance of charge, we also synthesized a sample with an Eu occupied Y site in the $CaYAlO_4$ host, as $CaY_{0.99}AlO_4$:$Eu_{0.01}$. However, there is no emission of Eu^{2+} in $CaY_{0.99}AlO_4$:$Eu_{0.01}$. The Ca^{2+} is highly overbonded with a bond valence sum (BVS) greater than +2 (∼+2.19) in the small Ca site calculated from the average structure Ca−O bond lengths from Rietveld refinement, indicating that the Ca site is highly compressed.[13] This situation is consistent with the fact that the CaO_9 polyhedron is surrounded compactly by AlO_6 octahedrons, as the crystal structure shows in Figure 1b. Moreover, the ionic radius of Eu^{2+} (^9r = 1.30 Å for 9-coordination) has a larger size than Ca^{2+} (^9r = 1.18 Å for 9-coordination).[49] Thus, it can be concluded that the local environment and size of the replaced crystal-site (Ca^{2+} in this system) play a dominant role in the reduction of Eu^{3+}.[12,50]

Through the crystal-site engineering approach, we introduced Si^{4+}−Ca^{2+} into the $CaYAlO_4$ host to replace Al^{3+}−Y^{3+} attempting to shrink the AlO_6 octahedrons, accompanied by the expansion of CaO_9 polyhedron, then fulfilling the conditions for the reduction of Eu^{3+}, because Si^{4+} has a smaller radius than Al^{3+} and substitution of Y^{3+} by Ca^{2+} can achieve charge compensation in the whole structure.[11,12,51] As the XRD pattern shows in Supporting Information Figure S3, impurities began to appear when *x* exceeded 0.30; thus, we restricted the *x* value to a maximum of 0.30. First, Rietveld refinement with GSAS program has been performed to reveal more details to clarify how substitution (Si^{4+}−Ca^{2+} for Al^{3+}−Y^{3+}) affects the $Ca_{0.99+x}Y_{1-x}Al_{1-x}Si_xO_4$:$Eu_{0.01}$ (CYASO, x = 0−0.30) crystal structure and luminescence properties. As shown in Supporting Information Figure S4, the observed, calculated, and difference results from the refinements are consistent with the Bragg positions, which indicate the formation of solid solution. The corresponding fine structure of CYASO:Eu (x = 0−0.30) is further examined by HRTEM as displayed in the inset of Supporting Information Figure S4, which presents a very uniform contrast without significant defects, indicating the high

DOI: 10.1021/am508859c
ACS Appl. Mater. Interfaces 2015, 7, 2715−2725

Table 2. Crystallographic Data and Reliability Factor of $Ca_{0.99+x}Y_{1-x}Al_{1-x}Si_xO_4$:$Eu_{0.01}$ (x = 0.05−0.30) Samples

	x = 0.05	x = 0.10	x = 0.15	x = 0.20	x = 0.30
$a = b$ (Å)	3.64722	3.64679	3.64587	3.64539	3.64477
c (Å)	11.88618	11.88631	11.88749	11.8901	11.89201
V (Å^3)	158.11	158.07	158.01	158.00	157.97
R_p	5.74%	5.51%	5.44%	5.88%	5.98%
R_{wp}	7.82%	7.58%	8.00%	8.38%	8.77%

crystallinity. Table 2 summarizes the lattice parameters and reliability factors of $Ca_{0.99+x}Y_{1-x}Al_{1-x}Si_xO_4$:$Eu_{0.01}$ (x = 0.05−0.30) samples. Obviously, the structure refinements converged with a final R_p of about 6% and R_{wp} of about 8%, which further prove the good quality of fit. From the lattice parameters and cell volumes for $Ca_{0.99+x}Y_{1-x}Al_{1-x}Si_xO_4$:$Eu_{0.01}$ (x = 0−0.30) samples obtained from Rietveld refinement analysis plotted in Figure 3, a gradual change in the lattice parameters with

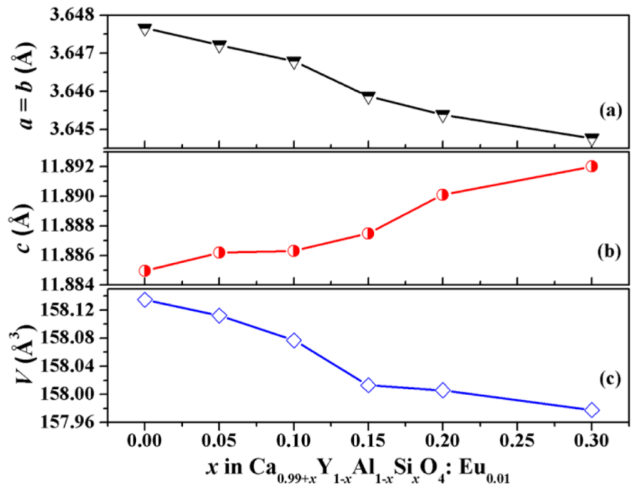

Figure 3. (a) Lattice parameters of a and b, (b) lattice parameters of c, and (c) cell volumes of $Ca_{0.99+x}Y_{1-x}Al_{1-x}Si_xO_4$:$Eu_{0.01}$ (x = 0−0.30) obtained from Rietveld refinement, reflecting the effects of the cation substitutions.

increasing x, a linear decrease in the a and b lattice parameters and an increase in the c lattice parameter, indicates that solid solutions are formed in $Ca_{0.99+x}Y_{1-x}Al_{1-x}Si_xO_4$:$Eu_{0.01}$ (x = 0−0.30). According to Vegard's rule, the sum of the ionic radii of the Si^{4+}−Ca^{2+} pair [$^6r(Si^{4+}) + {}^9r(Ca^{2+})$ = 0.40 Å + 1.18 Å = 1.58 Å] is smaller than that of the Al^{3+}−Y^{3+} pair in $CaYAlO_4$ parent structure [$^6r(Al^{3+}) + {}^9r(Y^{3+})$ = 0.535 Å + 1.075 Å = 1.61 Å].[12,49] Therefore, the unit cell contraction caused by the substitution of Al^{3+}−Y^{3+} by Si^{4+}−Ca^{2+} is presented in Figure 3c. However, the simultaneous contraction and expansion of the lattice parameters in different directions causes increased tilting of the AlO_6 octahedrons and greater distortion of the AlO_6 octahedrons and $(Ca/Y)O_9$ polyhedrons, which would greatly affect the local environment of activators and the corresponding luminescence properties as discussed in the following paragraphs.[13,52] In addition, the Raman spectrum, which is more sensitive to the cluster ordering, has been conducted to reveal the local ordering, deformation about site symmetry, etc.[53,54] As shown in Supporting Information Figure S5, the main phonon modes basically do not change with the introduction of Si^{4+}−Ca^{2+}, which is consistent with the XRD results. Furthermore, due to the fact that Ca^{2+} site is surrounded compactly by AlO_6 octahedrons, the ^{27}Al solid-state NMR spectra of CYASO:Eu (x = 0, 0.15, and 0.30) samples have been performed to further clarify the effect of incorporating Si^{4+}−Ca^{2+} on Ca^{2+} site as displayed in Figure 4. The intensity and fwhm of dominant

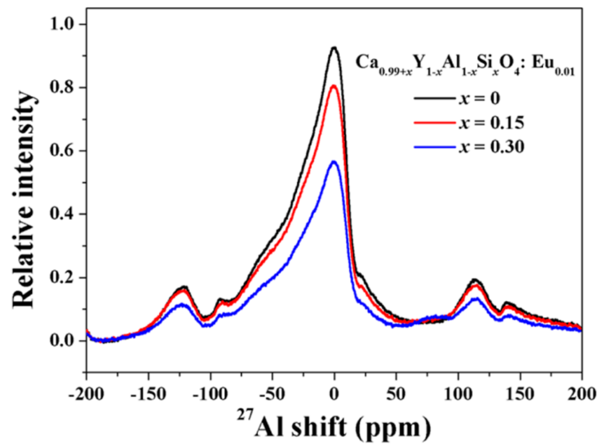

Figure 4. ^{27}Al solid-state NMR spectra of $Ca_{0.99+x}Y_{1-x}Al_{1-x}Si_xO_4$:$Eu_{0.01}$ (x = 0, 0.15, and 0.30) samples.

peak at 0.43 ppm in CYASO:Eu (x = 0, 0.15, and 0.30) samples decrease with increasing x, which is due to the reduction of the core ^{27}Al amount. Meanwhile, a weak peak appears at about 75 ppm in x = 0.15 and 0.30 samples.[24,45] Thus, it can be concluded that the local environment of activators was changed due to the introduction of Si^{4+}−Ca^{2+}, resulting in a loose site that is more suitable for Eu^{2+} occupation.

Figure 5a illustrates the emission spectra of $Ca_{0.99+x}Y_{1-x}Al_{1-x}Si_xO_4$:$Eu_{0.01}$ (x = 0−0.30) samples under the excitation of 277 nm. It is surprising to find an appearance of a broad band centered around 500 nm with increasing x, which can be assigned to the $4f^65d^1$−$4f^7$ transition of Eu^{2+}, accompanied by the intrinsic line emission of Eu^{3+} within the red range as discussed above.[15,55] Apparently, the luminescence intensity of Eu^{2+} increases with increasing x in the $Ca_{0.99+x}Y_{1-x}Al_{1-x}Si_xO_4$:$Eu_{0.01}$ (x = 0−0.30) system. Thus, the emissions of Eu^{3+} within 570−650 nm and Eu^{2+} centered about 500 nm emerge simultaneously, resulting in the emission colors change from red to yellow, as confirmed by the photographs and CIE coordinates listed in Figure 5b. This result suggests that Eu^{3+} is partially transformed to Eu^{2+} in the $Ca_{0.99+x}Y_{1-x}Al_{1-x}Si_xO_4$:$Eu_{0.01}$ (x = 0−0.30) system, which can be attributed to the increase of x value. Taking $Ca_{0.99+x}Y_{1-x}Al_{1-x}Si_xO_4$:$Eu_{0.01}$ (x = 0.15) for example, the PLE and PL spectra were systematically studied as shown in Figure 6. In the PLE spectrum monitored at 624 nm, which is produced by $^5D_0$−$^7F_2$ of Eu^{3+}, a strong broad band appears around 200−350 nm, which is ascribed to the charge transfer band (CTB) of O−Eu as mentioned above. Monitored at the wavelength of 503 nm, the PLE spectrum reveals a broad band from 250 to 450 nm with maximum at 335 nm, which can be

DOI: 10.1021/am508859c
ACS Appl. Mater. Interfaces 2015, 7, 2715−2725

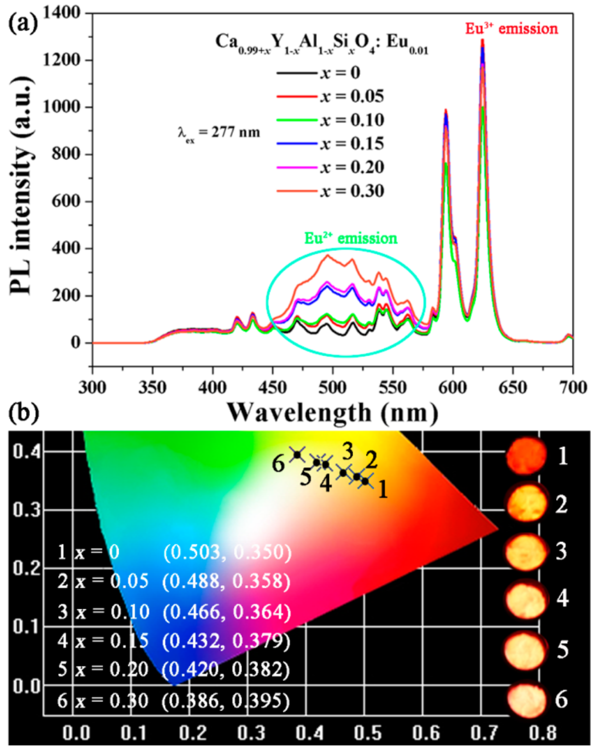

Figure 5. (a) PL spectra of $Ca_{0.99+x}Y_{1-x}Al_{1-x}Si_xO_4$:$Eu_{0.01}$ (x = 0–0.30) samples with changing x (λ_{ex} = 277 nm), and (b) the corresponding CIE coordinates and photographs.

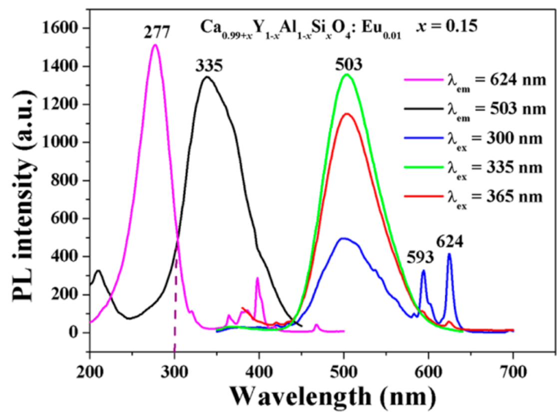

Figure 6. PLE and PL spectra of $Ca_{0.99+x}Y_{1-x}Al_{1-x}Si_xO_4$:$Eu_{0.01}$ (x = 0.15) sample.

ascribed to the $4f^7$–$4f^65d^1$ transition of the Eu^{2+} ions. It can be seen that the point of intersection of PLE spectrum between Eu^{2+} and Eu^{3+} is located at about 300 nm; thus, we can anticipate that the transitions of both Eu^{2+} ($4f^65d^1$–$4f^7$, broadband around 503 nm) and Eu^{3+} ($^5D_0$–$^7F_{1,2}$, 593 and 624 nm) could be obtained simultaneously under the 300 nm excitation, confirmed by the PL spectra (the blue line) shown in Figure 6. Under the excitation of 335 nm, the $Ca_{0.99+x}Y_{1-x}Al_{1-x}Si_xO_4$:$Eu_{0.01}$ (x = 0.15) phosphor produces a very broad symmetric emission band peaking at around 503 nm with the full-width at half-maximum (fwhm) of about 2883 cm^{-1}, which corresponds to the typical $4f^65d^1$–$4f^7$ transition of Eu^{2+} ion. Furthermore, no red line emission is detected under excitation of 335 nm, because Eu^{3+} has no absorption in this range as displayed in Supporting Information Figure S6.[12,56]

Upon the excitation with 365 nm, the line-emission of Eu^{3+} is much weaker than the band-emission of Eu^{2+} due to the fact that the absorption efficiency of Eu^{3+} is low in this range. In addition, XPS was applied to confirm the ionic states of Eu in the CYASO:Eu (x = 0 and 0.15) samples as shown in Supporting Information Figure S7. As compared to the dominant spin–orbit components Eu^{3+} $3d_{3/2}$ and $3d_{5/2}$ at around 1165 and 1135 eV in the x = 0 sample, the Eu^{2+} $3d_{3/2}$ and $3d_{5/2}$ configurations were clearly observed at around 1155 and 1126 eV in the x = 0.15 sample, which demonstrate the coexistence of Eu^{3+} and Eu^{2+}.[55] Luminescence decay curves of Eu^{2+} and Eu^{3+} in $Ca_{0.99+x}Y_{1-x}Al_{1-x}Si_xO_4$:$Eu_{0.01}$ (x = 0–0.30) have been performed, and the fitted curves for x = 0.15 sample have been shown in Figure 7 for simplicity. For Eu^{2+}, the

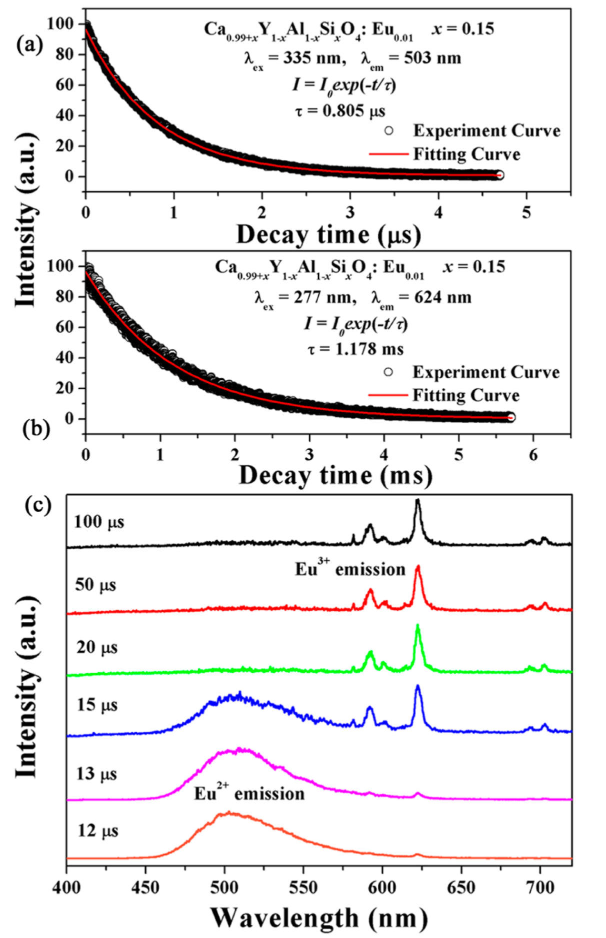

Figure 7. Decay curves of (a) Eu^{2+}: λ_{ex} = 335 nm, λ_{em} = 503 nm; (b) Eu^{3+}: λ_{ex} = 277 nm, λ_{em} = 624 nm; and (c) the corresponding time-resolved emission spectra of $Ca_{0.99+x}Y_{1-x}Al_{1-x}Si_xO_4$:$Eu_{0.01}$ (x = 0.15) sample.

lifetimes are 0.734, 0.791, 0.805, 0.845, and 0.769 μs, and for Eu^{3+}, the lifetimes are 1.156, 1.190, 1.167, 1.178, 1.153, and 1.148 ms, as listed in Supporting Information Table S1, respectively, basically agreeing well with previous reports (which further proves the coexistence of Eu^{2+} and Eu^{3+} activators).[57,58] Obviously, the lifetimes of Eu^{2+} and Eu^{3+} with different x values are in the same order of magnitude, which is consistent with the crystal structure of $CaYAlO_4$. By the time-resolved spectra, the Eu^{3+} luminescence can be distinctly separated from Eu^{2+}, as depicted in Figure 7c. Clearly, the emission spectra under short delay time (t = 12 and 13 μs)

DOI: 10.1021/am508859c
ACS Appl. Mater. Interfaces 2015, 7, 2715–2725

show a dominant band from Eu^{2+}. Under the delay time, 15 μs, the emissions of Eu^{2+} ($4f^65d^1-4f^7$ transition) and Eu^{3+} ($^5D_0-^7F_{0,1,2}$ transition) appear simultaneously. With prolonging the delay time (t = 100 μs), the emission of Eu^{2+} at 503 nm decreased obviously due to the short lifetime of Eu^{2+}, and the emission peaks corresponding to the $^5D_0-^7F_{0,1,2}$ transitions of Eu^{3+} became dominant in the $Ca_{0.99+x}Y_{1-x}Al_{1-x}Si_xO_4:Eu_{0.01}$ (x = 0.15) sample, indicative of the two valence states, +2 and +3, available for Eu ions.[18] Thus, it can be concluded that the reduction of Eu^{3+} to Eu^{2+} took place in the $Ca_{0.99+x}Y_{1-x}Al_{1-x}Si_xO_4:Eu_{0.01}$ (x = 0–0.30) system.

On the basis of refinements analysis, the effect of $Si^{4+}-Ca^{2+}$ incorporation involved in the Ca^{2+} sites can be analyzed by the bond lengths of (Al/Si)−O and (Ca/Y)−O, as shown in Figure 8. The (Al/Si)−O bond length decreases with increasing x in $Ca_{0.99+x}Y_{1-x}Al_{1-x}Si_xO_4:Eu_{0.01}$, which can be assigned to the Si^{4+} replacement of Al^{3+}. Consequently, the (Ca/Y)−O bond length is further elongated due to contraction of the $(Al/Si)O_6$ octahedron when incorporating Si^{4+}, thus loosening the crystal site of Ca^{2+}, which is favorable for Eu^{3+} to be reduced to Eu^{2+} in the Ca^{2+} sites. The polyhedral volumes were calculated as displayed in Figure 8c and d, the simultaneous contraction of the $(Al/Si)O_6$ and expansion of $(Ca/Y)O_9$ with increasing x, which is consistent with the variation tendency of the (Al/Si)−O and (Ca/Y)−O lengths.[13,59] Figure 8e and f shows the changing polyhedral distortion index (D) as x increases, based on the equation $D = 1/n\sum_{i=1}^{n}|(l_i-l_{av})/l_{av}|$, where l_i is the distance from the central atom to the ith coordinating atom and l_{av} is the average bond length. The distortion of the active sites where the Eu resides greatly affects the luminescence properties of the $Ca_{0.99+x}Y_{1-x}Al_{1-x}Si_xO_4:Eu_{0.01}$, as discussed later in this paper.[60] Bond valence sums (BVS) calculated from refinements results were adopted to help determine the microstructure of active sites, as shown in Figure 9.[61] Ca^{2+} is highly overbonded with a BVS greater than +2 (∼+2.19), while Y^{3+} is underbonded with a value (∼+2.52) smaller than +3. However, the sum of the BVS of Ca^{2+} and Y^{3+} is consistent with the optimum value (∼+5) presented in blue line of Figure 9. Considering the local environment of $(Ca/Y)O_9$ polyhedron, this structure causes one site to be overbonded and one site to be underbonded, while the intermediate compositions with varying Ca/Y ratios are able to balance this and achieve an optimized bonding network. Furthermore, the overbonded situation of Ca^{2+} sites can be alleviated by elongation of the Ca−O bond lengths, making the local environment of Eu more amenable to the optically active charge state of +2.[13,62]

As the scheme displayed in Figure 10a, the center Ca^{2+}/Y^{3+} ions are surrounded by coordinated O^{2-} ions that also linked

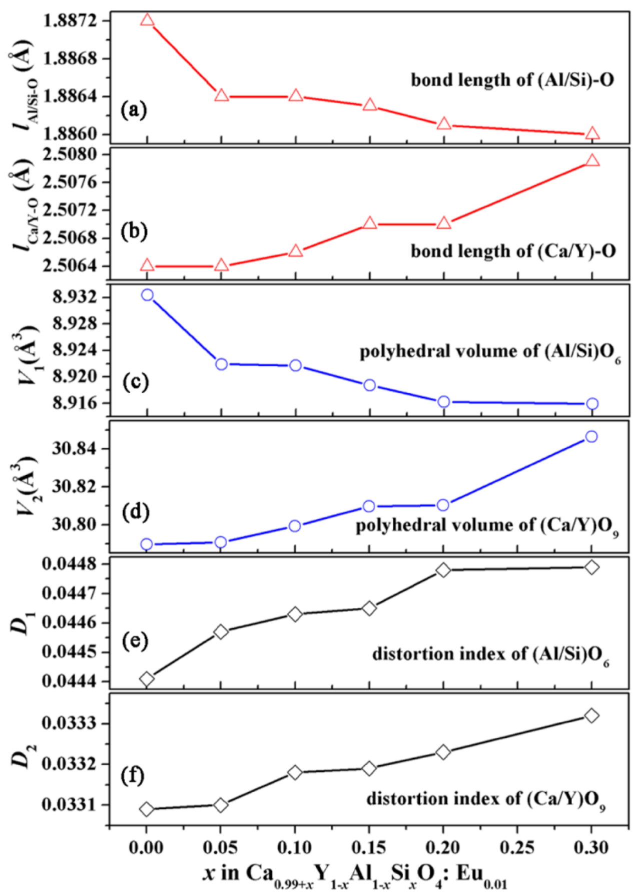

Figure 8. Average bond length of (a) (Al/Si)−O, (b) (Ca/Y)−O; the polyhedral volumes of (c) $(Al/Si)O_6$, (d) $(Ca/Y)O_9$, and the related distortion index (e and f) in $Ca_{0.99+x}Y_{1-x}Al_{1-x}Si_xO_4:Eu_{0.01}$ (x = 0–0.30) samples with changing x.

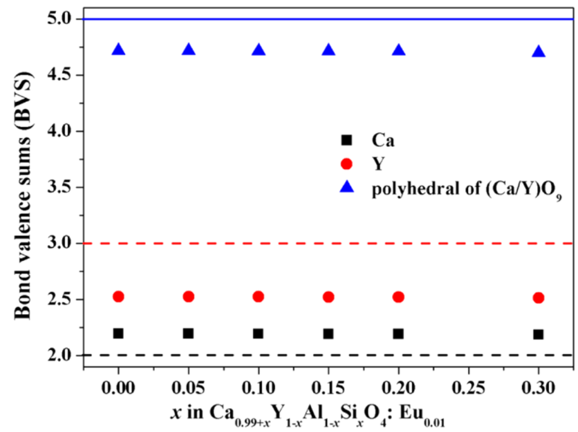

Figure 9. Bond valence sums (BVS) of Ca and Y atoms in the $Ca_{0.99+x}Y_{1-x}Al_{1-x}Si_xO_4:Eu_{0.01}$ (x = 0–0.30) systems.

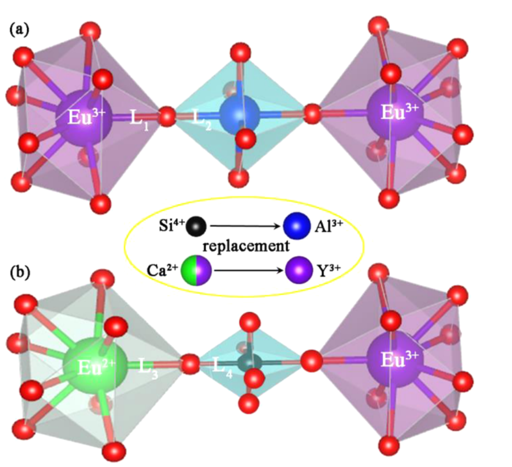

Figure 10. Local structural coordination of Eu ions in the lattices of (a) $CaYAlO_4:0.01Eu^{3+}$, (b) $Ca_{0.99+x}Y_{1-x}Al_{1-x}Si_xO_4:Eu_{0.01}$ (x = 0–0.30) series. The mixed-valence state of Eu activators at selected Ca^{2+} sites is proposed for the crystal-site engineering approach.

DOI: 10.1021/am508859c
ACS Appl. Mater. Interfaces 2015, 7, 2715−2725

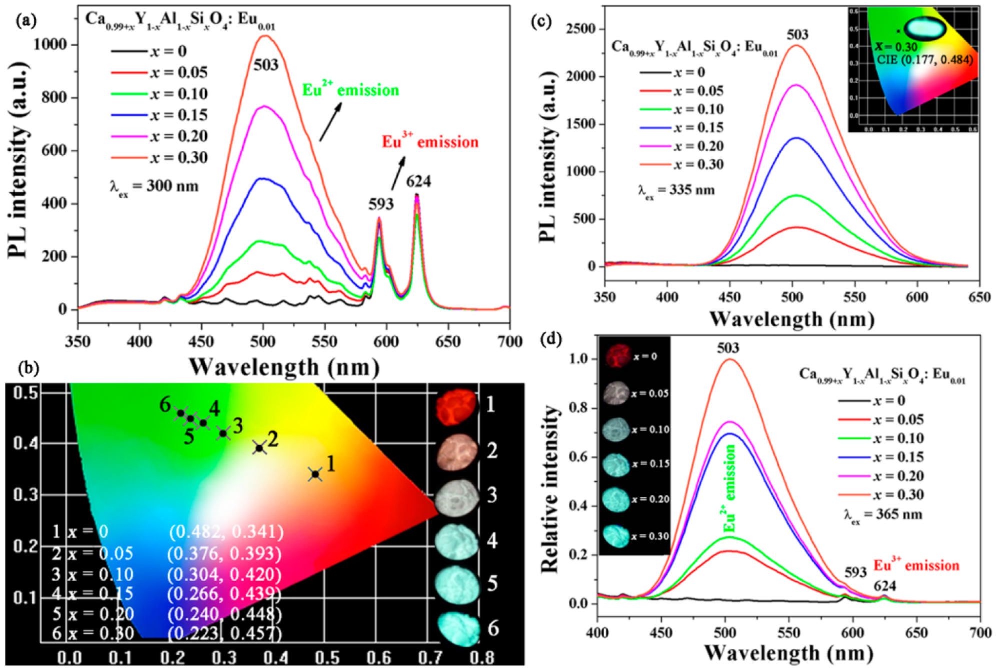

Figure 11. PL spectra and photographs of $Ca_{0.99+x}Y_{1-x}Al_{1-x}Si_xO_4$:$Eu_{0.01}$ (x = 0–0.30) samples with different excitation sources: (a, b) λ_{ex} = 300 nm, (c) λ_{ex} = 335 nm, and (d) λ_{ex} = 365 nm.

with other neighboring cations, such as Al^{3+}, Ca^{2+}, and Y^{3+} ions. The framework of $CaYAlO_4$ consists of AlO_6 octahedrons and $(Ca/Y)O_9$ polyhedrons connected with each other through sharing the O^{2-} vertexes. Upon introduction of activator ion, Eu^{3+} would randomly occupy Ca/Y sites in the host lattice. Because of the tilting of the AlO_6 octahedrons and highly compressed Ca/Y sites, Eu^{3+} is difficult to reduce to Eu^{2+}, resulting in the red emission of Eu^{3+}. On incorporation of Si^{4+}–Ca^{2+} in the $Ca_{0.99+x}Y_{1-x}Al_{1-x}Si_xO_4$:$Eu_{0.01}$ system, the central Y^{3+} cation is substituted by a Ca^{2+} cation with increasing x, while the neighboring Al^{3+} cation at the second shell is substituted by Si^{4+}, as presented in Figure 10b. Generally, the attractive force of the central cations toward the anions can be roughly evaluated by the ionic potential (φ), which can be calculated from $\varphi = Z/r$, where Z is the electric charge number of ion, and r is the ion radius (pm).[63,64] It can be obtained that $\varphi(Ca^{2+})$ = 0.0169, $\varphi(Y^{3+})$ = 0.0279, $\varphi(Si^{4+})$ = 0.10, and $\varphi(Al^{3+})$ = 0.056. Thus, $\varphi(Ca^{2+}) < \varphi(Y^{3+})$ and $\varphi(Si^{4+}) > \varphi(Al^{3+})$. When Al^{3+}–Y^{3+} is substituted by Si^{4+}–Ca^{2+}, the attractive force of the Ca^{2+}–O^{2-} becomes weaker; meanwhile, the attractive force of the Si^{4+}–O^{2-} becomes stronger, as compared to Y^{3+}–O^{2-} and Al^{3+}–O^{2-}, respectively. The bond length of Ca–O becomes longer ($L_3 > L_1$) and the bond length of Si–O becomes shorter ($L_4 < L_2$). Thus, the Ca^{2+} sites could be expanded through substitution of Al^{3+}–Y^{3+} by Si^{4+}–Ca^{2+}. Therefore, Eu^{3+} can be partially reduced to Eu^{2+} in the $Ca_{0.99+x}Y_{1-x}Al_{1-x}Si_xO_4$:$Eu_{0.01}$ lattice.

As shown in Figure 11a, the PL spectra of $Ca_{0.99+x}Y_{1-x}Al_{1-x}Si_xO_4$:$Eu_{0.01}$ (x = 0–0.30) exhibit both green emission of Eu^{2+} ($4f^65d^1$–$4f^7$, broadband around 503 nm) and red-orange emission of Eu^{3+} ($^5D_0$–$^7F_{1,2}$, 593 and 624 nm) upon excitation with 300 nm light. The PL intensity of Eu^{2+} increases with increasing x in the $Ca_{0.99+x}Y_{1-x}Al_{1-x}Si_xO_4$:$Eu_{0.01}$ (x = 0–0.30) system, indicating that the reduction process occurs easily with the gradual introduction of Si^{4+}–Ca^{2+}. As for the PL intensity of Eu^{3+}, things become complicated. On the one hand, the concentration of Eu^{3+} would be reduced due to the reduction process, which can decrease the PL intensity. On the other hand, the distortion index (D) of $(Ca/Y)O_9$ increases with increasing x, which would lower the symmetry of Eu^{3+} ions, thus increasing the PL intensity.[13,47] The same situation holds for the PLE spectra of Eu^{2+} (λ_{em} = 503 nm) and Eu^{3+} (λ_{em} = 624 nm) in the $Ca_{0.99+x}Y_{1-x}Al_{1-x}Si_xO_4$:$Eu_{0.01}$ (x = 0–0.30) system as shown in Supporting Information Figures S8 and S9. Because of the coexistence of Eu^{2+} and Eu^{3+}, the CIE coordinates upon 300 nm excitation of $Ca_{0.99+x}Y_{1-x}Al_{1-x}Si_xO_4$:$Eu_{0.01}$ (x = 0–0.30) are regularly shifted from (0.482, 0.341) to (0.223, 0.457) with increasing x as displayed in Figure 11b, and the inset shows the corresponding photographs of each composition irradiated under a 300 nm UV lamp. Maybe the sensitivity of eye to emission wavelength is different from the digital camera; thus, there is a little difference between the calculated CIE coordinates and the digital photographs. Especially for the $Ca_{0.99+x}Y_{1-x}Al_{1-x}Si_xO_4$:$Eu_{0.01}$ (x = 0.05) sample, the emission of Eu^{2+} and Eu^{3+} covers the whole visible region with comparable intensity, resulting in a light-yellow emission with CIE coordinates (x = 0.376, y = 0.393), which is located near the white light zone, indicating that this material can be used for WLEDs. In addition, we systematically measured the luminescence properties of Eu^{2+} and Eu^{3+}, such as quantum efficiency, I_{02}/I_{01} ratios, and Eu^{2+}/Eu^{3+} ratios, and the obtained results have been listed in Supporting Information Table S1. Furthermore, the I_{02}/I_{01} ratios of Eu^{3+} could be used as a probe to clarify the variation of local environment.[47] We believe that these parameters can help us to understand the change of coordination environment around Eu and the different luminescence properties of Eu^{2+}/Eu^{3+}. Under the excitation of 335 nm, the PL spectra of $Ca_{0.99+x}Y_{1-x}Al_{1-x}Si_xO_4$:$Eu_{0.01}$ (x = 0–0.30) only present the broad band emission of Eu^{2+}, resulting in a bright green emission, which can be confirmed by the photograph and CIE coordinates shown in the inset of Figure 11c. In addition, the PL intensity gradually increases with increasing value of x, which is correlated to the increasing

DOI: 10.1021/am508859c
ACS Appl. Mater. Interfaces 2015, 7, 2715–2725

level of Eu^{2+}, and the highest quantum yield is 55.6% as listed in Supporting Information Table S1. Because of the fact that the $4f^65d^1-4f^7$ transitions of Eu^{2+} ions are parity-allowed and sensitive to the crystal fields of the surrounding ions, this dependence on the crystal field enables tuning of the emission color easily through structure modification.[45,65−67] However, the normalized PL spectra of $Ca_{0.99+x}Y_{1-x}Al_{1-x}Si_xO_4$:$Eu_{0.01}$ (x = 0−0.30) varied little with changing the content of $Si^{4+}-Ca^{2+}$ because there exist two opposite effects, as shown in Supporting Information Figure S10. According to the equation $\Delta = Dq = Ze^2r^4/6R^5$, Dq is a measure of the crystal field strength, Z is the charge or valence of the anion, e is the charge of the electron, r is the radius of the d wave function, and R is the distance between the central ion and its ligands.[41,68] As mentioned above, the average bond lengths Ca−O increase when $Al^{3+}-Y^{3+}$ is substituted by $Si^{4+}-Ca^{2+}$; thus, the magnitude of the crystal field decreases, resulting in a blue-shift in emission. The polyhedral distortion index (D) is another important variable that influences on the emission energies. It is obvious that D of CaO_9 gradually increases with increasing x as displayed in Figure 8f. Previous work has shown that increasing polyhedral distortion may also increase the crystal field splitting and result in a red-shift in the PL properties.[13,52] As a net effect, the PL spectra position of $Ca_{0.99+x}Y_{1-x}Al_{1-x}Si_xO_4$:$Eu_{0.01}$ (x = 0−0.30) varied little with changing x. Similarly, the emission color of $Ca_{0.99+x}Y_{1-x}Al_{1-x}Si_xO_4$:$Eu_{0.01}$ (x = 0−0.30) could also be systematically tuned in a wide range through changing the value x upon 365 nm excitation, as the photographs of each composition show in Figure 11d, which further exhibit their potential application in WLEDs.

The thermal stability of phosphors is an important index for the practical application of WLEDs.[2,3] Temperature that is dependent on relative emission intensities for the $Ca_{0.99+x}Y_{1-x}Al_{1-x}Si_xO_4$:$Eu_{0.01}$ x = 0.30 sample under 335 nm excitation in the temperature range of 0−150 °C is compared in Figure 12a. It is obvious that the luminescence intensity decreases with increasing of temperature and there is only emission of Eu^{2+} under excitation of 335 nm even when the temperature is increased to 150 °C; thus, we can conclude that Eu^{2+} is stable in this host. Specifically, the emission band has a slight blue shift toward the higher energy side as shown in Figure 12b. This phenomenon can be ascribed to the thermally active phonon-assisted tunneling from the excited states of the lower-energy emission band to those of the high-energy emission band in the configuration coordinate diagram.[15] After absorption of the excitation energy, undesirable non-radiative relaxation (phonons) occurs; meanwhile, emission takes place at the bottom of the excited state by radiative transitions.[24] However, under high temperature, thermal activation can happen due to the electron−phonon coupling, and the energy reaches the crossing point between the excited and ground states. In this case, nonradiative relaxation occurs by heat dissipation rather than radiation emission, which could quench the luminescence.[15,17]

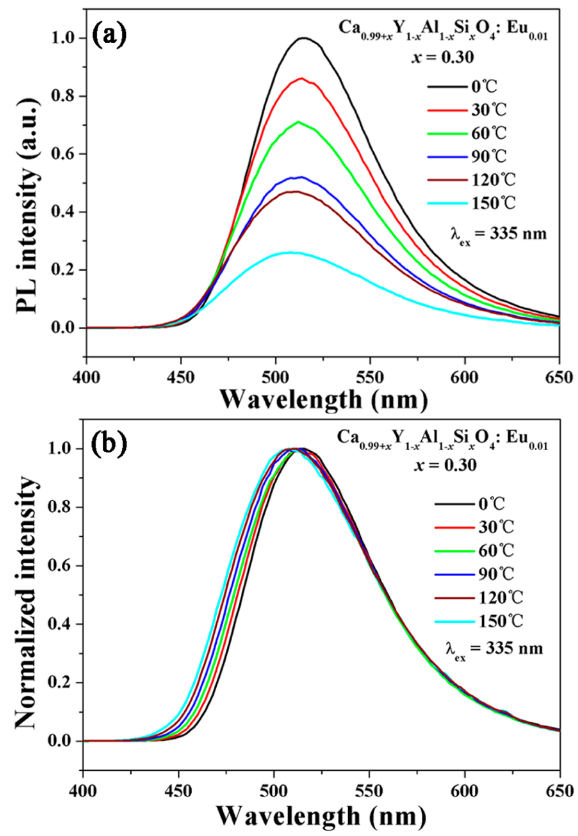

Figure 12. (a) Relative PL intensity and (b) normalized PL spectra of $Ca_{0.99+x}Y_{1-x}Al_{1-x}Si_xO_4$:$Eu_{0.01}$ x = 0.30 sample with different temperatures, λ_{ex} = 335 nm.

4. CONCLUSIONS

In summary, we have successfully prepared a series of $Ca_{0.99+x}Y_{1-x}Al_{1-x}Si_xO_4$:$Eu_{0.01}$ (x = 0−0.30) phosphors with the coexistence of Eu^{2+} and Eu^{3+} using the crystal-site engineering approach. The Rietveld refinement analysis presents that the average bond lengths of Al−O and Ca−O are systematically shortened and elongated, respectively, indicating that the enlargement of activator site is fulfilled by the replacement of $Al^{3+}-Y^{3+}$ by $Si^{4+}-Ca^{2+}$, which plays a dominant role in the reduction of Eu^{3+}. Incorporation $Si^{4+}-Ca^{2+}$ in CYASO:Eu phosphor leads to a broad green emission band centered around 503 nm, which can be ascribed to the $4f^65d^1-4f^7$ transition of Eu^{2+} ions. In addition, the relative intensity of Eu^{2+} and Eu^{3+} could be easily tuned through changing x, resulting in tunable emission colors in a wide range, which is beneficial to improve the illumination quality. Because of the broad PLE spectrum (ranging from 250 to 450 nm) and tunable luminescence (Eu^{2+} and Eu^{3+}), this phosphor holds great promise for application in WLEDs. Furthermore, this crystal-site engineering approach is promising for obtaining novel phosphor materials because only a single activator Eu can generate the multiband emission by optical combination of different valences of europium. In addition, detailed information on the relationships between active site size and polyhedron shape and PL properties will facilitate the discovery of novel phosphors suitable for lighting and display applications.

■ ASSOCIATED CONTENT

Ⓢ Supporting Information

XRD patterns of (a) $CaYAlO_4$:$0.01Eu^{3+}$ and (b) Y_2O_3 (JCPDS 20-1412); (a) the TEM image, (b) HRTEM image, (c) the fast Fourier transform (FFT) images, and (d) the selected area electron diffraction (SAED) pattern of $CaYAlO_4$:$0.01Eu^{3+}$, indicating the high crystalline nature of the sample. XRD patterns for $Ca_{0.99+x}Y_{1-x}Al_{1-x}Si_xO_4$:$Eu_{0.01}$ x = 0.35 and the standard data of $CaYAlO_4$ (JCPDS 24-0221). Rietveld refinement to XRD patterns for $Ca_{0.99+x}Y_{1-x}Al_{1-x}Si_xO_4$:$Eu_{0.01}$

DOI: 10.1021/am508859c
ACS Appl. Mater. Interfaces 2015, 7, 2715−2725

with different doping concentrations of x of (a) $x = 0.05$, (b) $x = 0.10$, (c) $x = 0.15$, (d) $x = 0.20$, and (e) $x = 0.30$, respectively, with the insets as the corresponding HRTEM images. Raman spectra of $Ca_{0.99+x}Y_{1-x}Al_{1-x}Si_xO_4:Eu_{0.01}$ (x = 0−0.30) samples. PLE spectrum of $Ca_{0.99+x}Y_{1-x}Al_{1-x}Si_xO_4:Eu_{0.01}$ (x = 0.15) sample (λ_{em} = 624 nm). XPS spectra of Eu in $Ca_{0.99+x}Y_{1-x}Al_{1-x}Si_xO_4:Eu_{0.01}$ (a) x = 0 and (b) x = 0.15. PLE spectra of $Ca_{0.99+x}Y_{1-x}Al_{1-x}Si_xO_4:Eu_{0.01}$ (x = 0−0.30) samples with changing x (λ_{em} = 503 nm). PLE spectra of $Ca_{0.99+x}Y_{1-x}Al_{1-x}Si_xO_4:Eu_{0.01}$ (x = 0−0.30) samples with changing x (λ_{em} = 624 nm). Normalized PL spectra of $Ca_{0.99+x}Y_{1-x}Al_{1-x}Si_xO_4:Eu_{0.01}$ (x = 0−0.30) samples with changing x (λ_{ex} = 335 nm). Luminescence parameters of $Ca_{0.99+x}Y_{1-x}Al_{1-x}Si_xO_4:Eu_{0.01}$ (x = 0−0.30) samples. This material is available free of charge via the Internet at http://pubs.acs.org.

AUTHOR INFORMATION

Corresponding Authors

*E-mail: mmshang@ciac.ac.cn.

*E-mail: jlin@ciac.ac.cn.

Notes

The authors declare no competing financial interest.

ACKNOWLEDGMENTS

This project is financially supported by the National Natural Science Foundation of China (Grants NSFC 91433110, 51472234, 51332008), the National Basic Research Program of China (Grant 2010CB327704), and the Joint Funds of the National Natural Science Foundation of China and Guangdong Province (Grant U1301242).

REFERENCES

(1) Höppe, H. A. Recent Developments in the Field of Inorganic Phosphors. *Angew. Chem., Int. Ed.* **2009**, *48*, 3572−3582.

(2) McKittrick, J.; Shea-Rohwer, L. E. Review: Down Conversion Materials for Solid-State Lighting. *J. Am. Ceram. Soc.* **2014**, *97*, 1327−1352.

(3) George, N. C.; Denault, K. A.; Seshadri, R. Phosphors for Solid-State White Lighting. *Annu. Rev. Mater. Res.* **2013**, *43*, 481−501.

(4) Ye, S.; Xiao, F.; Pan, Y. X.; Ma, Y. Y.; Zhang, Q. Y. Phosphors in Phosphor-Converted White Light-Emitting Diodes: Recent Advances in Materials, Techniques and Properties. *Mater. Sci. Eng., R* **2010**, *71*, 1−34.

(5) Li, X.; Budai, J. D.; Liu, F.; Howe, J. Y.; Zhang, J.; Wang, X.-J.; Gu, Z.; Sun, C.; Meltzer, R. S.; Pan, Z. New Yellow $Ba_{0.93}Eu_{0.07}Al_2O_4$ Phosphor for Warm-White Light-Emitting Diodes Through Single-Emitting-Center Conversion. *Light Sci. Appl.* **2013**, *2*, e50.

(6) Matioli, E.; Brinkley, S.; Kelchner, K. M.; Hu, Y.-L.; Nakamura, S.; DenBaars, S.; Speck, J.; Weisbuch, C. High-Brightness Polarized Light-Emitting Diodes. *Light Sci. Appl.* **2012**, *1*, e22.

(7) Oh, J. H.; Yang, S. J.; Do, Y. R. Healthy, Natural, Efficient and Tunable Lighting: Four-Package White LEDs for Optimizing the Circadian Effect, Color Quality and Vision Performance. *Light Sci. Appl.* **2014**, *3*, e141.

(8) Xie, R. J. Optical Properties of (Oxy) Nitride Materials: A Review. *J. Am. Ceram. Soc.* **2013**, *96*, 665−687.

(9) Park, W. B.; Singh, S. P.; Sohn, K.-S. Discovery of a Phosphor for Light Emitting Diode Applications and Its Structural Determination, $Ba(Si,Al)_5(O,N)_8:Eu^{2+}$. *J. Am. Chem. Soc.* **2014**, *136*, 2363−2373.

(10) Pust, P.; Weiler, V.; Hecht, C.; Tücks, A.; Wochnik, A. S.; Henß, A.-K.; Wiechert, D.; Scheu, C.; Schmidt, P. J.; Schnick, W. Narrow-Band Red-Emitting $Sr[LiAl_3N_4]:Eu^{2+}$ as a Next-Generation LED-Phosphor Material. *Nat. Mater.* **2014**, *13*, 891−896.

(11) Sato, Y.; Kato, H.; Kobayashi, M.; Masaki, T.; Yoon, D.-H.; Kakihana, M. Tailoring the Deep-Red Luminescence in $Ca_2SiO_4:Eu^{2+}$. *Angew. Chem., Int. Ed.* **2014**, *53*, 7756−7759.

(12) Huang, K. W.; Chen, W. T.; Chu, C. I.; Hu, S. F.; Sheu, H. S.; Cheng, B. M.; Chen, J. M.; Liu, R. S. Controlling Activator Site to Tune Europium Valence in Oxyfluoride Phosphors. *Chem. Mater.* **2012**, *24*, 2220−2227.

(13) Denault, K. A.; Brgoch, J.; Gaultois, M. W.; Mikhailovsky, A.; Petry, R.; Winkler, H.; DenBaars, S. P.; Seshadri, R. Consequences of Optimal Bond Valence on Structural Rigidity and Improved Luminescence Properties in $Sr_xBa_{2-x}SiO_4:Eu^{2+}$ Orthosilicate Phosphors. *Chem. Mater.* **2014**, *26*, 2275−2282.

(14) Grzyb, T.; Szczeszak, A.; Rozowska, J.; Legendziewicz, J.; Lis, S. Tunable Luminescence of $Sr_2CeO_4:M^{2+}$ (M = Ca, Mg, Ba, Zn) and $Sr_2CeO_4:Ln^{3+}$ (Ln = Eu, Dy, Tm) Nanophosphors. *J. Phys. Chem. C* **2012**, *116*, 3219−3226.

(15) Ci, Z.; Que, M.; Shi, Y.; Zhu, G.; Wang, Y. Enhanced Photoluminescence and Thermal Properties of Size Mismatch in $Sr_{2.97-x-y}Eu_{0.03}Mg_xBa_ySiO_5$ for High-Power White Light-Emitting Diodes. *Inorg. Chem.* **2014**, *53*, 2195−2199.

(16) Hao, J.; Cocivera, M. Luminescent Characteristics of Blue-Emitting $Sr_2B_5O_9Cl$: Eu Thin-Film Phosphors. *Appl. Phys. Lett.* **2001**, *79*, 740−742.

(17) Liu, C.; Qi, Z.; Ma, C.-G.; Dorenbos, P.; Hou, D.; Zhang, S.; Kuang, X.; Zhang, J.; Liang, H. High Light Yield of $Sr_8(Si_4O_{12})Cl_8:Eu^{2+}$ under X-ray Excitation and Its Temperature-Dependent Luminescence Characteristics. *Chem. Mater.* **2014**, *26*, 3709−3715.

(18) Xie, H.; Lu, J.; Guan, Y.; Huang, Y.; Wei, D.; Seo, H. J. Abnormal Reduction, $Eu^{3+}\rightarrow Eu^{2+}$, and Defect Centers in Eu^{3+}-Doped Pollucite, $CsAlSi_2O_6$, Prepared in an Oxidizing Atmosphere. *Inorg. Chem.* **2014**, *53*, 827−834.

(19) Xia, Z.; Liu, R.-S.; Huang, K.-W.; Drozd, V. $Ca_2Al_3O_6F:Eu^{2+}$: a Green-Emitting Oxyfluoride Phosphor for White Light-Emitting Diodes. *J. Mater. Chem.* **2012**, *22*, 15183−15189.

(20) Liu, Y.; Tu, D.; Zhu, H.; Chen, X. Lanthanide-Doped Luminescent Nanoprobes: Controlled Synthesis, Optical Spectroscopy, and Bioapplications. *Chem. Soc. Rev.* **2013**, *42*, 6924−6958.

(21) Wang, P.; Wang, Y.; Tong, L. Functionalized Polymer Nanofibers: a Versatile Platform for Manipulating Light at the Nanoscale. *Light Sci. Appl.* **2013**, *2*, e102.

(22) Zhang, Z. J.; ten Kate, O. M.; Delsing, A.; Stevens, M. J. H.; Zhao, J. T.; Notten, P. H. L.; Dorenbos, P.; Hintzen, H. T. Photoluminescence Properties of Yb^{2+} in $CaAlSiN_3$ as a Novel Red-Emitting Phosphor for White LEDs. *J. Mater. Chem.* **2012**, *22*, 23871−23876.

(23) Wang, X.-M.; Wang, C.-H.; Wu, M. M.; Wang, Y. X.; Jing, X.-P. O/N Ordering in the Structure of $Ca_3Si_2O_4N_2$ and the Luminescence Properties of the Ce^{3+} Doped Material. *J. Mater. Chem.* **2012**, *22*, 3388−3394.

(24) Li, G.; Lin, C. C.; Chen, W.-T.; Molokeev, M. S.; Atuchin, V. V.; Chiang, C.-Y.; Zhou, W.; Wang, C.-W.; Li, W.-H.; Sheu, H.-S.; Chan, T.-S.; Ma, C.; Liu, R.-S. Photoluminescence Tuning via Cation Substitution in Oxonitridosilicate Phosphors: DFT Calculations, Different Site Occupations, and Luminescence Mechanisms. *Chem. Mater.* **2014**, *26*, 2991−3001.

(25) Zhang, Y.; Geng, D.; Kang, X.; Shang, M.; Wu, Y.; Li, X.; Lian, H.; Cheng, Z.; Lin, J. Rapid, Large-Scale, Morphology-Controllable Synthesis of $YOF:Ln^{3+}$ (Ln = Tb, Eu, Tm, Dy, Ho, Sm) Nano-/Microstructures with Multicolor-Tunable Emission Properties. *Inorg. Chem.* **2013**, *52*, 12986−12994.

(26) Liu, X.; Li, C.; Quan, Z.; Cheng, Z.; Lin, J. Tunable Luminescence Properties of $CaIn_2O_4$: Eu^{3+} Phosphors. *J. Phys. Chem. C* **2007**, *111*, 16601−16607.

(27) Wang, Y.; Brik, M. G.; Dorenbos, P.; Huang, Y.; Tao, Y.; Liang, H. Enhanced Green Emission of Eu^{2+} by Energy Transfer from the $^5D_3$ Level of Tb^{3+} in $NaCaPO_4$. *J. Phys. Chem. C* **2014**, *118*, 7002−7009.

(28) Zhang, Y.; Kang, X.; Geng, D.; Shang, M.; Wu, Y.; Li, X.; Lian, H.; Cheng, Z.; Lin, J. Highly Uniform and Monodisperse $GdOF:Ln^{3+}$ (Ln = Eu, Tb, Tm, Dy, Ho, Sm) Microspheres: Hydrothermal

DOI: 10.1021/am508859c
ACS Appl. Mater. Interfaces 2015, 7, 2715−2725

Synthesis and Tunable-Luminescence Properties. *Dalton Trans.* **2013**, *42*, 14140−14148.
(29) Morozov, V. A.; Bertha, A.; Meert, K. W.; Van Rompaey, S.; Batuk, D.; Martinez, G. T.; Van Aert, S.; Smet, P. F.; Raskina, M. V.; Poelman, D.; Abakumov, A. M.; Hadermann, J. Incommensurate Modulation and Luminescence in the $CaGd_{2(1-x)}Eu_{2x}(MoO_4)_{4(1-y)}(WO_4)_{4y}$ ($0 \leq x \leq 1$, $0 \leq y \leq 1$) Red Phosphors. *Chem. Mater.* **2013**, *25*, 4387−4395.
(30) Su, Y.; Li, L.; Li, G. Synthesis and Optimum Luminescence of $CaWO_4$-Based Red Phosphors with Codoping of Eu^{3+} and Na^+. *Chem. Mater.* **2008**, *20*, 6060−6067.
(31) Ji, H.; Huang, Z.; Xia, Z.; Molokeev, M. S.; Atuchin, V. V.; Fang, M.; Huang, S. New Yellow-Emitting Whitlockite-Type Structure $Sr_{1.75}Ca_{1.25}(PO_4)_2$:$Eu^{2+}$ Phosphor for Near-UV Pumped White Light-Emitting Devices. *Inorg. Chem.* **2014**, *53*, 5129−5135.
(32) Pust, P.; Wochnik, A. S.; Baumann, E.; Schmidt, P. J.; Wiechert, D. U.; Scheu, C.; Schnick, W. Ca[$LiAl_3N_4$]: Eu^{2+}-A Narrow Band Red-Emitting Nitridolithoaluminate. *Chem. Mater.* **2014**, *26*, 3544−3549.
(33) Yu, J.; Hao, Z.; Zhang, X.; Luo, Y.; Zhang, J. A new Emission Band of Eu^{2+} and Its Efficient Energy Transfer to Mn^{2+} in $Sr_2Mg_3P_4O_{15}$:Mn^{2+}, Eu^{2+}. *Chem. Commun.* **2011**, *47*, 12376−12378.
(34) Setlur, A. A.; Radkov, E. V.; Henderson, C. S.; Her, J.-H.; Srivastava, A. M.; Karkada, N.; Kishore, M. S.; Kumar, N. P.; Aesram, D.; Deshpande, A. Energy-efficient, High-Color-Rendering LED Lamps Using Oxyfluoride and Fluoride Phosphors. *Chem. Mater.* **2010**, *22*, 4076−4082.
(35) Mao, Z.-y.; Wang, D.-j.; Lu, Q.-f.; Yu, W.-h.; Yuan, Z.-h. Tunable Single-Doped Single-Host Full-Color-Emitting $LaAlO_3$:Eu Phosphor-via Valence State-Controlled Means. *Chem. Commun.* **2009**, 346−348.
(36) Mao, Z.-y.; Wang, D.-j. Tuning of Direct White Light of Lanthanum Aluminate with Mixed-Valence Europium. *Inorg. Chem.* **2010**, *49*, 4922−4927.
(37) Geng, D.; Li, G.; Shang, M.; Peng, C.; Zhang, Y.; Cheng, Z.; Lin, J. Nanocrystalline CaYAlO4: Tb^{3+}/Eu^{3+} as Promising Phosphors for Full-Color Field Emission Displays. *Dalton Trans.* **2012**, *41*, 3078−3086.
(38) Guille, A.; Pereira, A.; Breton, G.; Bensalah-Ledoux, A.; Moine, B. Energy Transfer in CaYAlO4: Ce^{3+}, Pr^{3+} for Sensitization of Quantum-cutting with the Pr^{3+}-Yb^{3+} Couple. *J. Appl. Phys.* **2012**, *111*, 043104.
(39) Ryba-Romanowski, W.; Gołąb, S.; Hanuza, J.; Mączka, M.; Pietraszko, A.; Berkowski, M.; Pajączkowska, A. Optical Study of $CaNdAlO_4$. *J. Phys. Chem. Solids* **1991**, *52*, 1043−1049.
(40) Lv, S.; Zhu, Z.; Wang, Y.; You, Z.; Li, J.; Tu, C. Spectroscopic Investigations of Ho^{3+}/Er^{3+}: $CaYAlO_4$ and Eu^{3+}/Er^{3+}: $CaYAlO_4$ Crystals for 2.7 μm Emission. *J. Lumin.* **2013**, *144*, 117−121.
(41) Guille, A.; Pereira, A.; Martinet, C.; Moine, B. Quantum Cutting in $CaYAlO_4$: Pr^{3+}, Yb^{3+}. *Opt. Lett.* **2012**, *37*, 2280−2282.
(42) Zandi, B.; Merkle, L.; Hutchinson, J.; Verdun, H.; Chai, B. Upconversion and Energy Transfer Modeling in Er, Yb: $CaYAlO_4$. *J. Phys. IV* **1994**, *4*, C4−587-C4−590.
(43) Larson, A. C.; Von Dreele, R. B. GSAS Report; Los Alamos, NM, 1994; pp 86−748.
(44) Shannon, R.; Oswald, R.; Parise, J.; Chai, B.; Byszewski, P.; Pajaczkowska, A.; Sobolewski, R. Dielectric Constants and Crystal Structures of $CaYAlO_4$, $CaNdAlO_4$, and $SrLaAlO_4$, and Deviations from the Oxide Additivity Rule. *J. Solid State Chem.* **1992**, *98*, 90−98.
(45) George, N. C.; Pell, A. J.; Dantelle, G.; Page, K.; Llobet, A.; Balasubramanian, M.; Pintacuda, G.; Chmelka, B. F.; Seshadri, R. Local Environments of Dilute Activator Ions in the Solid-State Lighting Phosphor $Y_{3-x}Ce_xAl_5O_{12}$. *Chem. Mater.* **2013**, *25*, 3979−3995.
(46) Im, W. B.; Fellows, N. N.; DenBaars, S. P.; Seshadri, R.; Kim, Y. I. $LaSr_2AlO_5$, a Versatile Host Compound for Ce^{3+}-Based Yellow Phosphors: Structural Tuning of Optical Properties and Use in Solid-State White Lighting. *Chem. Mater.* **2009**, *21*, 2957−2966.
(47) Yu, M.; Lin, J.; Fang, J. Silica Spheres Coated with YVO_4: Eu^{3+} Layers via Sol-Gel Process: A Simple Method to Obtain Spherical Core-Shell Phosphors. *Chem. Mater.* **2005**, *17*, 1783−1791.
(48) Gwak, S. J.; Arunkumar, P.; Im, W. B. A New Blue-Emitting Oxohalide Phosphor Sr_4OCl_6:Eu^{2+} for Thermally Stable, Efficient White-Light-Emitting Devices under Near-UV. *J. Phys. Chem. C* **2014**, *118*, 2686−2692.
(49) Shannon, R. D. Revised Effective Ionic Radii and Systematic Studies of Interatomic Distances in Halides and Chalcogenides. *Acta Crystallogr., Sect. A* **1976**, *32*, 751−767.
(50) Huang, C.-H.; Wu, P.-J.; Lee, J.-F.; Chen, T.-M. (Ca,Mg,Sr)$_9$Y-$(PO_4)_7$:Eu^{2+},Mn^{2+}: Phosphors for White-light Near-UV LEDs through Crystal Field Tuning and Energy Transfer. *J. Mater. Chem.* **2011**, *21*, 10489−10495.
(51) Im, W. B.; George, N.; Kurzman, J.; Brinkley, S.; Mikhailovsky, A.; Hu, J.; Chmelka, B. F.; DenBaars, S. P.; Seshadri, R. Efficient and Color-Tunable Oxyfluoride Solid Solution Phosphors for Solid-State White Lighting. *Adv. Mater.* **2011**, *23*, 2300−2305.
(52) Denault, K.; Paden, S.; Brinkley, S.; Mikhailovsky, A. A.; Neuefeind, J. C.; DenBaars, S. P.; Seshadri, R. A Green-Yellow Emitting Oxyfluoride Solid Solution Phosphor Sr_2Ba-$(AlO_4F)_{1-x}(SiO_5)_x$: Ce^{3+} for Thermally Stable, High Color Rendition Solid State White Lighting. *J. Mater. Chem.* **2012**, *22*, 18204−18213.
(53) Mahesh, S. K.; Rao, P. P.; Thomas, M.; Francis, T. L.; Koshy, P. Influence of Cation Substitution and Activator Site Exchange on the Photoluminescence Properties of Eu^{3+}-Doped Quaternary Pyrochlore Oxides. *Inorg. Chem.* **2013**, *52*, 13304−13313.
(54) Zhang, Y.; Geng, D.; Li, X.; Fan, J.; Li, K.; Lian, H.; Shang, M.; Lin, J. Wide-Band Excited $YTiTaO_6$: Eu^{3+}/Er^{3+} Phosphors: Structure Refinement, Luminescence Properties, and Energy Transfer Mechanisms. *J. Phys. Chem. C* **2014**, *118*, 17983−17991.
(55) Kim, M. A.; Lee, S. J.; Jung, J.; Park, J. K. A Facile Reduction of Eu^{3+} to Eu^{2+} in Gadolinium Monosulfide Nanoparticles Using a Mixed Solvent of Oleic Acid/Hexadecylamine. *Chem. Commun.* **2012**, *48*, 904−906.
(56) Kanji Patel, D.; Sengupta, A.; Vishwanadh, B.; Sudarsan, V.; Kumar Vatsa, R.; Kadam, R.; Kumar Kulshreshtha, S. Local Environments Around Eu^{3+} and Eu^{2+} Ions in Dual Light-Emitting $BaSnO_3$: Eu Nanomaterials. *Eur. J. Inorg. Chem.* **2012**, *2012*, 1609−1619.
(57) Zhang, Y.; Li, X.; Geng, D.; Shang, M.; Lian, H.; Cheng, Z.; Lin, J. YOF Nano/Micro-Crystals: Morphology Controlled Hydrothermal Synthesis and Luminescence Properties. *CrystEngComm* **2014**, *16*, 2196−2204.
(58) Lee, G.-y.; Han, J. Y.; Im, W. B.; Cheong, S. H.; Jeon, D. Y. Novel Blue-Emitting $Na_xCa_{1-x}Al_{2-x}Si_{2+x}O_8$:$Eu^{2+}$ ($x = 0.34$) Phosphor with High Luminescent Efficiency for UV-Pumped Light-Emitting Diodes. *Inorg. Chem.* **2012**, *51*, 10688−10694.
(59) Swanson, D. K.; Peterson, R. C. Polyhedral Volume Calculations. *Can. Mineral.* **1980**, *18*, 153−156.
(60) Baur, W. The Geometry of Polyhedral Distortions Predictive Relationships for the Phosphate Group. *Acta Crystallogr., Sect. B* **1974**, *30*, 1195−1215.
(61) Brese, N.; O'keeffe, M. Bond-Valence Parameters for Solids. *Acta Crystallogr., Sect. B: Struct. Sci.* **1991**, *47*, 192−197.
(62) Im, W. B.; Brinkley, S.; Hu, J.; Mikhailovsky, A.; DenBaars, S. P.; Seshadri, R. $Sr_{2.975-x}Ba_xCe_{0.025}AlO_4F$: A Highly Efficient Green-Emitting Oxyfluoride Phosphor for Solid State White Lighting. *Chem. Mater.* **2010**, *22*, 2842−2849.
(63) Zhang, Y.; Wu, Z.; Geng, D.; Kang, X.; Shang, M.; Li, X.; Lian, H.; Cheng, Z.; Lin, J. Full Color Emission in $ZnGa_2O_4$: Simultaneous Control of the Spherical Morphology, Luminescent, and Electric Properties via Hydrothermal Approach. *Adv. Funct. Mater.* **2014**, *24*, 6581−6593.
(64) Zhang, Q.; Wang, J.; Zhang, M.; Ding, W.; Su, Q. Enhanced Photoluminescence of $Ca_2Al_2SiO_7$: Eu^{3+} by Charge Compensation Method. *Appl. Phys. A: Mater. Sci. Process.* **2007**, *88*, 805−809.
(65) Seibald, M.; Rosenthal, T.; Oeckler, O.; Fahrnbauer, F.; Tücks, A.; Schmidt, P. J.; Schnick, W. Unexpected Luminescence Properties of $Sr_{0.25}Ba_{0.75}Si_2O_2N_2$:$Eu^{2+}$-A Narrow Blue Emitting Oxonitridosilicate with Cation Ordering. *Chem.—Eur. J.* **2012**, *18*, 13446−13452.

DOI: 10.1021/am508859c
ACS Appl. Mater. Interfaces 2015, 7, 2715−2725

(66) Huang, W.-Y.; Yoshimura, F.; Ueda, K.; Shimomura, Y.; Sheu, H.-S.; Chan, T.-S.; Chiang, C.-Y.; Zhou, W.; Liu, R.-S. Chemical Pressure Control for Photoluminescence of $MSiAl_2O_3N_2:Ce^{3+}/Eu^{2+}$ (M = Sr, Ba) Oxynitride Phosphors. *Chem. Mater.* **2014**, *26*, 2075−2085.
(67) Park, J.; Lee, S. J.; Kim, Y. J. Evolution of Luminescence of $Sr_{2-y-z}Ca_zSi(O_{1-x}N_x)_4:yEu^{2+}$ with N^{3-}, Eu^{2+}, and Ca^{2+} Substitutions. *Cryst. Growth Des.* **2013**, *13*, 5204−5210.
(68) Dorenbos, P. Energy of the First $4f^7 \rightarrow 4f^6 5d$ Transition of Eu^{2+} in Inorganic Compounds. *J. Lumin.* **2003**, *104*, 239−260.

DOI: 10.1021/am508859c
ACS Appl. Mater. Interfaces 2015, 7, 2715−2725